Aerosol Science and Technology
Publication details, including instructions for authors and subscription information:
http://www.tandfonline.com/loi/uast20

Simulating and Modeling Particulate Removal Processes by Elliptical Fibers

Haoming Wang [a] , Haibo Zhao [a] , Kun Wang [a] & Chuguang Zheng [a]
[a] State Key Laboratory of Coal Combustion , Huazhong University of Science and Technology , Wuhan , Hubei , People's Republic of China
Accepted author version posted online: 26 Nov 2013.Published online: 26 Dec 2013.

To cite this article: Haoming Wang , Haibo Zhao , Kun Wang & Chuguang Zheng (2014) Simulating and Modeling Particulate Removal Processes by Elliptical Fibers, Aerosol Science and Technology, 48:2, 207-218, DOI: 10.1080/02786826.2013.868595

To link to this article: http://dx.doi.org/10.1080/02786826.2013.868595

Aerosol Science and Technology, 48:207–218, 2014

ISSN: 0278-6826 print / 1521-7388 online
DOI: 10.1080/02786826.2013.868595

Simulating and Modeling Particulate Removal Processes by Elliptical Fibers

Haoming Wang, Haibo Zhao, Kun Wang, and Chuguang Zheng
State Key Laboratory of Coal Combustion, Huazhong University of Science and Technology, Wuhan, Hubei, People's Republic of China

A lattice Boltzmann-cellular automata (LB-CA) probabilistic model for two-phase flows was used to simulate the particle capture process of elliptical fiber. The pressure drop and capture efficiency due to various capture mechanisms (Brownian diffusion, interception, and inertial impaction) were investigated. It is found that the diffusional capture efficiency of the elliptical fiber is greater than that of the circular fiber because of its larger capture area, which is proportional to the aspect ratio. When the interception or inertial impaction is dominated, aspect ratio, orientation angle, and the ratio of particle diameter to the fiber diameter affect the capture efficiency of the elliptical fiber, which is usually higher than that of the circular fiber except that the major axis is parallel to the incoming flow. The correction factors for the pressure drop and capture efficiency of elliptical fiber from those of circular fiber were attained through the Levenberg–Marquardt algorithm, which is used to fit some well-organized LB-CA simulations. These empirical correction factors can combine the classical models for circular fiber to calculate the pressure drop and capture efficiency for elliptical fiber in a simple way. Finally, the quality factors of elliptical fibers as a function of the aspect ratio and orientation angle were investigated, which is conducive to optimization configuration of elliptical fiber in different operation conditions.

INTRODUCTION

Fibrous filter is at advantage of high removal efficiency for submicron particles, and it has been widely used in the fields of energy, environment, and chemical engineering (e.g., pulverized coal-fired power plant, mining engineering, and cement industry). Due to complicated particle–flow–fiber interactions and various particle capture mechanisms (Brownian diffusion, interception, inertial impaction, gravitational settling, and electrostatic attraction), a large amount of theoretical analysis, experimental measurements, and numerical simulations have been carried out for the quantitative picture of the filtration process.

At the early stage, almost all of researches focused on the fiber with a circular cross-section (circular fiber). By the use of the cell model, Kuwabara (1959) and Happel (1959) independently derived an analytical solution of the flow field (viscous Stokes flow around a circle) and attained the theoretical formula of drag force on single cylindrical fibers oriented perpendicular to the air flow. Starting from a good description of these idealized flow fields, many researchers (Stechkina and Fuchs 1966; Kirsch and Fuchs 1967, 1968; Stechkina et al. 1969; Lee and Liu 1982; Liu and Wang 1997) proposed analytical expressions for the pressure drop and diffusion/interception/impaction-dominated capture efficiency. Along with the development of new instruments for direct measurement of fibrous filter efficiencies, systematic experimental data are available (Lee and Liu 1981; Kasper et al. 2010). These experimental measurements are useful to understand the complex processes better, to attain empirical/semi-empirical formulas, and to validate/correct these analytical expressions. The development of computational fluid dynamics (CFD) also provides a promising way to simulate gas–solid two-phase flows in complex geometries. Numerical simulations have been developed for the filtration processes of particles with various diameter distribution by nanofibers or microfibers with different arrangement modes (Maze et al. 2007; Tahir and Tafreshi 2009; Hosseini and Tafreshi 2010a,b; Dunnett and Clement 2012).

Generally speaking, the filtration processes of filters composed of cylindrical fiber have been comprehensively studied, and some formulas for capture efficiency and pressure drop have been validated and been applied in engineering for the filtration prediction. However, only a few investigations have been dedicated to explore the filtration performance of filters made of noncircular fibers. Actually, synthetic fibers can be made with a variety of shape such as square, rectangular, elliptical, trilobal even "+", "T," and "O" hollow-shaped cross-section (Ushe 1993; William and Bobby 1995; Homonoff and Dugan 2001; Sanchez et al. 2007; Hosseini and Tafreshi 2011).

Several groups have studied the flow fields and pressure drop for the fibers with square and rectangular cross section using the

Received 15 May 2013; accepted 28 October 2013.
Address correspondence to Haibo Zhao, State Key Laboratory of Coal Combustion, Huazhong University of Science and Technology, Luoyu Road 1037, Wuhan, Hubei 430074, People's Republic of China. E-mail: klinsmannzhb@163.com
Color versions of one or more of the figures in the article can be found online at www.tandfonline.com/uast.

theoretical analysis and numerical simulation methods. Here, we quote the studies of Brown (1984), Fardi and Liu (1992a), Wang (1996), Ouyang and Liu (1998), and Dhaniyala (1999) for flow field and pressure drop, and Fardi and Liu (1992b) for capture efficiencies due to Brownian diffusion and interception, Zhu et al. (2000) for capture efficiency due to inertial impaction, and Adamiak (1999), Cao et al. (2004) and Cheung et al. (2005) for the filtration performance in an electric field. Hosseini and Tafreshi (2011) investigated the effects of fibers' cross-sectional shape on the performance of a nanofiber filter (in the slip flow regime) and a microfiber filter (in the no-slip flow regime).

Compared with rectangular and square fibers, elliptical fibers have rarely been studied in terms of flow fields, capture efficiency, and pressure drop. In fact, fibers with elliptical cross-section can offer bigger surface area per unit volume than usually used cylindrical fibers, and thus have performance advantages in the capture efficiency of submicron particles over circular fibers (Masliyah 1975). Furthermore, the elliptical fibers with a more streamlined shape exhibit less drag force than other fibers with square, circular, and trilobal cross sections (Hosseini and Tafreshi 2011).

In order to research the capture efficiency and pressure drop of elliptical fibers, the flow fields around elliptical fibers should be first obtained. Kuwabara (1959) first calculated the velocity field for a lattice of elliptical cylinders in a uniform flow at small Reynolds number using Oseen's approximation and then predicted the drag force and pressure drop. Brown (1984) calculated the velocity field and pressure drop for arrays of elliptical fibers with major axes either perpendicular or parallel to the incoming flow using numerical simulation methods. Raynor (2002) proposed analytical expressions for flow field around elliptical fibers and the aerodynamic drag and lift on the fibers using the cell model. However, the drag force by Raynor (2002) is quite different from that of Kuwabara (1959), Brown (1984), and Kirsh (2011), especially for the ratio of drag forces at the normal and parallel locations of the major axes relative to the flow. Some semi-empirical expressions for diffusional and interceptive efficiencies of single elliptical fiber were developed by Raynor and his colleagues (Raynor 2008; Regan and Raynor 2009). More recently, Wang et al. (2012b) calculated the velocity field of potential flow around an elliptical fiber based on Zhukovsky conversion, and then investigated the interception efficiency. They found that the elliptical fiber can improve obviously the interception efficiency of larger particles. Besides the analytical procedure, the CFD simulation was adopted to investigated filtration by elliptical fibers. Wang and Pui (2009) calculated the drag force and single-fiber efficiencies due to interception, inertial impaction, and Brownian diffusion in the case of two-dimensional staggered array configuration.

To sum up, the above-cited researches on elliptical filter fibers exhibit the following limitations. First, the presented analytical/ semi-empirical/empirical expressions for the capture efficiency and drag force (pressure drop) of elliptical fibers are very complicated and difficult to apply in engineering. Second, no quantitative expression for the impaction capture efficiency is available. Third, the relationship between the filtration performance of elliptical fiber and that of circular fiber is not clear. Fourth, there is no report on how the elliptical fiber collects particles due to diffusion, interception, and inertial impaction, since these existing researches only calculated the particle concentration fields or analyzed the flow field streamline to predict particle removal/deposition. Fifth, although the qualitative picture of the influence of fiber geometric properties and filtration condition on the filtration performance is physically reasonable, the quantitative situation is still not satisfactory.

We established a quantitative cellular-automata probabilistic model to describe the movement of particles on regular grid under external forces, and successfully simulated the steady-state and non-steady-state filtration processes by single circular fiber (Wang et al. 2012a). By comparing the simulation results of the lattice Boltzmann-cellular automatic probabilistic (LB-CA) model with previous theoretical predictions and experimental observations for the traditional filtration process, the LB-CA model is well validated. Good performance of the LB-CA model provides an opportunity to investigate the filtration process of noncircular fibers, like fibers with elliptical cross-section in this article. The LB-CA method is very suitable for simulating gas–solid two-phase flows around such irregular geometrical boundary (ellipse in this article). This article focuses on the simulation and modeling of the steady-state filtration processes of a single elliptical fiber, which is believed to the basis of the non-steady-state filtration processes of real filters composed of randomly distributed fibers. Our simulation covers three most important collection mechanisms: Brownian diffusion, interception, and inertial impaction. The pressure drop (in terms of dimensionless drag force acting on the fibers) and single-fiber efficiencies due to the three mechanisms are calculated and compared to these existing analytical/empirical/semi-empirical expressions and numerical results. We develop empirical expressions for the pressure drop and capture efficiencies of elliptical fibers based on these theoretical expressions for circular fibers. These empirical expressions are relatively simple and can be easily applied to predict the filtration performance. Thanks to the Lagrangian tracking nature of the LB-CA method, detailed information of the filtration processes is also obtained.

LB–CA METHOD FOR PARTICLE-LADEN FLOWS

Lattice Boltzmann (LB) Method for Flow Field

In the LB method, it is assumed that fluid consists of microscopic fictitious fluid particles. The state of each grid is presented by the distribution function $f_i(x,t)$ which indicates the probability density of the fictitious fluid particles that locate on lattice x with the velocity $\mathbf{c}_i$ at time t. The fictitious fluid particles on regular lattices have to experience two sequential substeps as

follows:

$$\text{Collision: } f_i(x,t)' = f_i(x,t) + \Omega_i, \quad [1]$$

$$\text{Streaming: } f_i(x + \mathbf{c}_i \cdot \Delta t, t + \Delta t) = f_i(x,t)', \quad [2]$$

where Ω_i is the collision operator. By combining two equations and introducing Bhatnagar–Gross–Krook (BG.K single-relaxation) collision operator (Bhatnagar et al. 1954), the evolution equation of the fluid system is obtained (Qian et al. 1992):

$$f_i(x+\mathbf{c}_i\cdot\Delta t, t+\Delta t) - f_i(x,t) = [f_i^{\text{eq}}(x,t) - f_i(x,t)]/\tau, \quad [3]$$

where Δt is time step, τ is the dimensionless relaxation time, and f_i^{eq} is the equilibrium distribution function. For simplicity and without loss of generality, we choose the two-dimensional square lattice with nine velocities $\mathbf{c}_i$ (*D2Q9* model, see Figure 1, i runs from 0 to 8):

$$\mathbf{c}_i = \begin{cases} (0,0) & i = 0 \\ c\left(\cos\left[(i-1)\frac{\pi}{2}\right], \sin\left[(i-1)\frac{\pi}{2}\right]\right) & i = 1,2,3,4 \\ \sqrt{2}c\left(\cos\left[(i-1)\frac{\pi}{2}\right], \sin\left[(i-1)\frac{\pi}{2}\right]\right) & i = 5,6,7,8 \end{cases}. \quad [4]$$

Then, the equilibrium distribution function can be calculated in the *D2Q9* model as follows:

$$f_i^{\text{eq}} = \rho\alpha_i\left[1 + \frac{\mathbf{c}_i\cdot\mathbf{u}}{c_s^2} + \frac{1}{2}\left(\frac{\mathbf{c}_i\cdot\mathbf{u}}{c_s^2}\right)^2 - \frac{\mathbf{u}^2}{2c_s^2}\right], \quad [5]$$

where $\mathbf{u}$ is the macroscopic velocity of local fluid, ρ is the fluid density, α_i is the weight coefficient related to the model with $\alpha_0 = 4/9$, $\alpha_i = 1/9$ ($i = 1, 3, 5, 7$) and $\alpha_i = 1/36$ ($i = 2, 4, 6, 8$) in the *D2Q9* model, c_s is the local sound speed, $c_s = \sqrt{3}c/3$, and $c = \Delta x/\Delta t$.

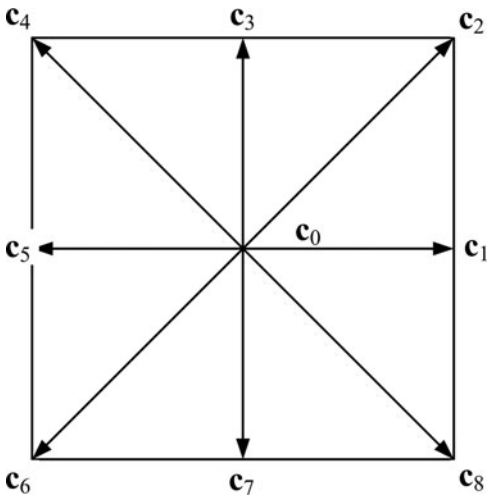

FIG. 1. Discrete velocities in *D2Q9* model.

The macroscopic quantities of flow fields can be derived from statistics of the distribution function, and the macroscopic density ρ and momentum $\rho\mathbf{u}$ are calculated as follows:

$$\rho = \sum_{i=0}^{Q-1} f_i,\ \rho\mathbf{u} = \sum_{i=0}^{Q-1} f_i\mathbf{c}_i. \quad [6]$$

The equations for calculating the fluid viscosity and pressure are given by

$$\begin{cases} \nu = \frac{c_s^2}{2}(2\tau - 1)\cdot\Delta t \\ P = \rho c_s^2 \end{cases}. \quad [7]$$

Cellular-Automata (CA) Probabilistic Model for Particle Motion

We established a quantitative LB-CA model (Wang et al. 2012a), in which the particles move on the same lattice as flow field with a probability (p_i) defined as the ratio of projected length of actual displacement in four directions ($\mathbf{e}_1$,$\mathbf{e}_3$,$\mathbf{e}_5$,$\mathbf{e}_7$) to grid length. Certainly, it must make sure that p_i is always nonnegative:

$$p_i = \max\left(0, \frac{\Delta x_{\text{p}}\cdot\mathbf{e}_i}{\Delta x}\right), (i = 1,3,5,7), \quad [8]$$

where Δx is the grid length, and Δx_{p} is the actual displacement of the particle within time step Δt. Finally, the particle position after one time step is calculated as

$$\mathbf{x}_{\text{p}}^{n+1} = \mathbf{x}_{\text{p}}^{n} + \mu_1\mathbf{e}_1 + \mu_3\mathbf{e}_3 + \mu_5\mathbf{e}_5 + \mu_7\mathbf{e}_7, \quad [9]$$

where μ_i is a Boolean variable equal to 1 with the probability p_i.

It is noticed that the key of the CA probabilistic model is to obtain Δx_{p} in Equation (8). In general, the particle motion is described by the Newtonian equation under consideration of external forces. During the filtration process of fibers, besides the drag force of particles caused by the flow fields, the random Brownian diffusion also exists. Therefore, the random Brownian force (Maze et al. 2007; Hosseini and Tafreshi 2010a) is used here to describe the random Brown diffusion motion of the particles, and the governing equation of particles are (only drag force and Brownian force are considered) written as

$$\frac{\mathrm{d}\mathbf{u}_{\text{p}}}{\mathrm{d}t} = \frac{\mathbf{u} - \mathbf{u}_{\text{p}}}{\tau_{\text{p}}} + \varsigma\sqrt{\frac{216\mu k_{\text{B}}T}{\pi\rho_{\text{p}}^2 d_{\text{p}}^5\Delta t}} \quad [10]$$

$$\frac{\mathrm{d}\mathbf{x}_{\text{p}}}{\mathrm{d}t} = \mathbf{u}_{\text{p}}, \quad [11]$$

where $\mathbf{u}_p$ is the particle velocity, τ_p is the particle relaxation timescale with $\tau_p = \rho_p {d_p}^2/(18\mu)$, μ is the gas kinetic viscosity, ς is the Gaussian random number with zero mean and a standard deviation of one, d_p is the particle diameter, k_B is the Boltzmann constant, and T is the temperature. The second term on the right-hand side of Equation (10) is the Brownian force.

Through twice integration of Equation (10) over time t, the particle velocity and displacement can be obtained respectively as follows:

$$\mathbf{u}_p^{n+1} = \mathbf{u}_p^n \cdot \exp\left(-\frac{\Delta t}{\tau_p}\right) + (\mathbf{u}_f + \mathbf{F}_B \cdot \tau_p) \cdot \left(1 - \exp\left(-\frac{\Delta t}{\tau_p}\right)\right) \quad [12]$$

$$\mathbf{x}_p^{n+1} = \mathbf{x}_p^n + \left(\mathbf{u}_p^n - \mathbf{u}_f\right)\left(1 - \exp\left(-\frac{\Delta t}{\tau_p}\right)\right) \cdot \tau_p + \mathbf{u}_f \cdot \Delta t + \left(\Delta t + \left(1 - \exp\left(-\frac{\Delta t}{\tau_p}\right)\right) \cdot \tau_p\right) \cdot \mathbf{F}_B \cdot \tau_p, \quad [13]$$

where superscript n represents the present moment and $n+1$ represents the next moment. Thus, the actual displacement $\Delta x_p (= \mathbf{x}_p^{n+1} - \mathbf{x}_p^n)$ of the particle within time step Δt is obtained, and the particle position can be determined by Equations (8) and 9.

For more model details (including boundary conditions), readers could refer to our recent publications (Wang et al. 2012a, 2013).

FLOW FIELD AND DATA PROCESSING METHOD

Flow Field

The elliptical fiber is placed in the center of a square computational domain. Assume that a, b, and θ respectively represent the length of major axes, minor axes, and orientation angle (the angle between major axes and streamwise). The aspect ratio ε equals to a:b and characteristic length d_f is defined as $(ab)^{1/2}$. The grid resolution is 256 × 256. The grid independence has been tested for circular fiber ($\varepsilon = 1$) under the same condition of this work. Three different grid resolutions (128 × 128, 256 × 256, and 512 × 512) were considered and then it is found that the 256 × 256 is sufficient to obtain accurate results.

Once the steady-state flow field is achieved, particles are injected from the left of the computational domain. During the filtration process, particles will be captured once it collides with fibers. The collected particles will "disappear" in the steady-state filtration processes, so the shape of fiber does not change and the fiber keeps "clean." Fiber capture efficiency can be calculated as follows:

$$\eta = \frac{G_1 - G_2}{G_1} \times 100\%, \quad [14]$$

where G_1 is the total number of solid particles entering the computational domain from the left inlet (monodisperse particles are considered in this article); G_2 is the total number of particles leaving the computational domain from the right outlet.

The inlet velocity of fluid is constant, $u(y) = u_0$, and it is considered that the initial velocity of particles in the inlet is the same as the fluid velocity. The upper and lower boundaries are considered to be periodic, that is, a fluid particle or a solid particle moving out the domain from the upper or lower boundary will enter into the domain from the opposite boundary at once. In this situation, the assumption of uniform inlet velocity profile is reasonable. On the other hand, although the particle velocity is different from the fluid velocity especially for the large-inertia particles, the assumption of the inlet particle velocity same as the fluid velocity has negligible effect on the simulation results because there is still an enough long distance for gas–solid flow to evolve before the particle is collected by the fiber. In the outlet, the flow field is regarded as fully developed, that is, $\partial u/\partial x = \partial v/\partial x = 0$. Nonequilibrium extrapolation scheme is used here to deal with inlet and outlet boundary conditions (Guo et al. 2002).

Levenberg–Marquardt Algorithm

In order to obtain a series of correction factors for the pressure drop and capture efficiency of the elliptical fiber based on the existing formulas of circular fiber, we utilize the Levenberg–Marquardt algorithm to fit some well-organized LB-CA simulations for quantitative prediction of the filtration performance of elliptical fiber. The Levenberg–Marquardt algorithm (LMA; More 1978) provides a numerical solution to minimize a nonlinear function (local minimum). This algorithm, which modifies the uncertain parameters of the function continuously, combines the advantages of the Gauss–Newton algorithm and the gradient descent method, and overcomes the shortcomings of the two methods. With respect to the Gauss–Newton method, it has the advantages that it is relatively efficient due to the determined direction and step size, and second derivatives are not required. However, it is difficult to convergence if initial estimates are far from the minimum. The two main advantages of the gradient descent method lie in the fact that it is guaranteed to find the minimum through numerous times of iterations as long as it exists and the very low storage requirements necessary. The disadvantages of the gradient descent method are that it tends to zigzag along the bottom of long narrow canyons and approaches the best-fit value very slowly.

The principle of LMA is: if f is a nonlinear mapping from $\mathbf{R}^m$ to $\mathbf{R}^n$, $x_i \in \mathbf{R}^m$ and $y_i \in \mathbf{R}^n$, then $f(x_i, \gamma) = y_i$, where γ_i is the uncertain coefficient. The purpose of the LMA is to find γ_i to minimize $\sum [y_i - f(x_i, \gamma)]^2$. Like other numerical minimization algorithms, the LMA is executed in an iterative procedure. To start a minimization, one obtains the following approximate equation through Taylor expansion of $f(x+\delta_x)$:

$$f(x_i, \gamma + \delta) \approx f(x_i, \gamma) + \mathbf{J}\delta, \quad [15]$$

where $\mathbf{J} = \partial f(x_i, \gamma)/\partial\gamma$. In each iteration step, it is assumed that iterative point is γ, then one needs to find a δ to minimize

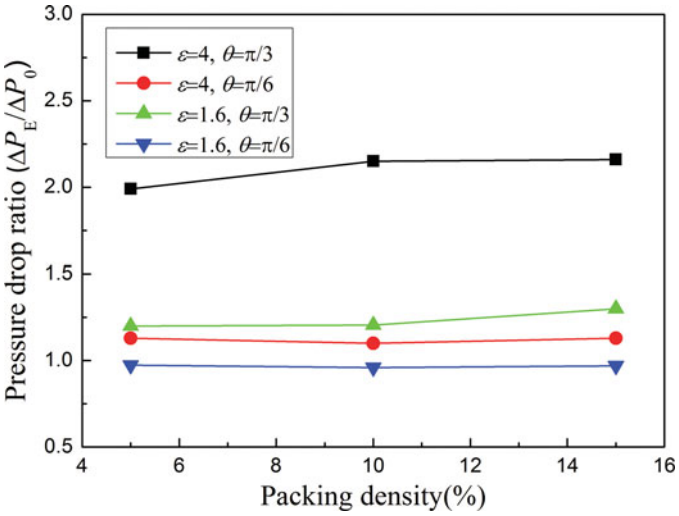

FIG. 2. Pressure drop ratio of elliptical to circular fiber vs. packing density.

the error of the following equation:

$$|y - f(\gamma + \delta)| \approx |y - f(\gamma) - \mathbf{J}\delta| = |\sigma - \mathbf{J}\delta|, \qquad [16]$$

where $\sigma = y - f(\gamma)$. According to the projection formula, the minimum error is attained when the following requirement is met:

$$\left[\lambda \mathbf{I} + \left(\mathbf{J}^{\mathrm{T}}\mathbf{J}\right)\right]\delta = \mathbf{J}^{\mathrm{T}}\left[y - f(\gamma)\right]. \qquad [17]$$

Once the value of δ is obtained, γ is updated as $\gamma+\delta$. The new value of γ is regarded as the initial value of the next iteration step. The iteration process is terminated when one of the following conditions is reached: the change of σ or δ is smaller than the prespecified value; the iteration number exceeds the limited value.

It is imagined that the pressure drop and capture efficiency of elliptical fibers depend on the following parameters: packing density α (the ratio of the cross-sectional area of the elliptical fiber to the area of calculation domain), aspect ratio ε, orientation angle θ, and the ratio of particle diameter and the fiber diameter $d_{\mathrm{p}}/d_{\mathrm{f}}$. In this article, the LMA is used to obtain several correction factors based on the existing classical formulas of the pressure drop and capture efficiency for circular fiber. In such a way, the existing formulas for circular fiber can be applied in the filtration prediction of elliptical fibers by considering the influence of α, ε, θ, and $d_{\mathrm{p}}/d_{\mathrm{f}}$.

PRESSURE DROP

The Effect of Fiber Packing Density on Pressure Drop

In order to investigate the relation between pressure drop and the three parameters (packing density, aspect ratio, and orientation angle), we first analyze the effect of the packing density on the pressure drop. As shown in Figure 2, the pressure drop ratio of an elliptical fiber (where aspect ratio and orientation angle are fixed) to circular fiber is almost independent of the packing density (5%–15%). It is noted that, in our simulation, the number of lattices is insufficient to describe accurately the shape of the elliptical fiber when α is too small. On the other hand, a large α may lead to the border of ellipse goes beyond the boundaries of the computational domain. So such range of packing density is selected in the article. The independence of packing density on the pressure drop ratio means that the correction factor of the pressure drop depends only on the aspect ratio and orientation angle. In other words, we can first fix the packing density to investigate the pressure drop as a function of ε and θ, and the resultant correction factor is suitable for other conditions of different packing densities.

Pressure Drop of Elliptical Fiber

Pressure drop of fiber filter is often characterized by dimensionless drag force acting on per unit length of fiber. Kuwabara (1959) gained the analytical expression of dimensionless drag force F_0 for circular fiber:

$$F_0 = 4\pi\left[-0.5\ln\alpha - 0.75 - 0.25\alpha^2 + \alpha\right]^{-1}. \qquad [18]$$

For the circular fiber, the drag force mainly depends on the fiber packing density. However, for elliptic fibers, the drag force is more complex. Even for the cases that the packing density is same, different aspect ratio or orientation angle leads to different drag forces of elliptical fiber. Aspect ratio and orientation angle determine the friction surface area and windward area of the fiber, respectively. In this section, a correction factor $C_{\mathrm{E,F}}(=F_{\mathrm{E}}/F_0)$ is obtained through fitting numerical simulation of the LB-CA model using the LMA, and it can be used to calculate the drag force on the elliptical fibers with different aspect ratio or orientation angle based on the existing expression (Equation (18)) for the circular fiber: $F_{\mathrm{E}} = C_{\mathrm{E,F}} \cdot F_0$.

Figure 3 shows the dimensionless drag force on elliptical fibers with the same packing density (=4.95% here). It is found from Figure 3a that, (1) when $\theta = 0$ (i.e., the long axial is parallel to the incoming flow), the dimensionless drag force becomes smaller at first and then gradually increases as ε increases. The observation coincides with the CFD simulation results of Wang and Pui (2009); (2) when $\theta > 0$ (i.e., $\theta = \pi/6, \pi/3, \pi/2$ in Figure 3a), the dimensionless drag force increases with the increase of ε. In fact, the dimensionless drag force is determined simultaneously by the windward area and the friction area, which both depend on θ and ε. When $\theta = 0$ and ε is small, the windward area has greater impact on F_{E} than the friction area. With the increase of ε, the windward area becomes smaller (on the contrary, the friction area becomes larger), therefore F_{E} reduces gradually. However, when ε increases to a certain extent, the friction area is predominant and then F_{E} increases. When $\theta = 0$ and $\varepsilon = 2.5$, the balance between the windward area and the friction area results in the minimum F_{E}. Figure 3b shows that, for a given ε, F_{E} increases with the increase of θ obviously.

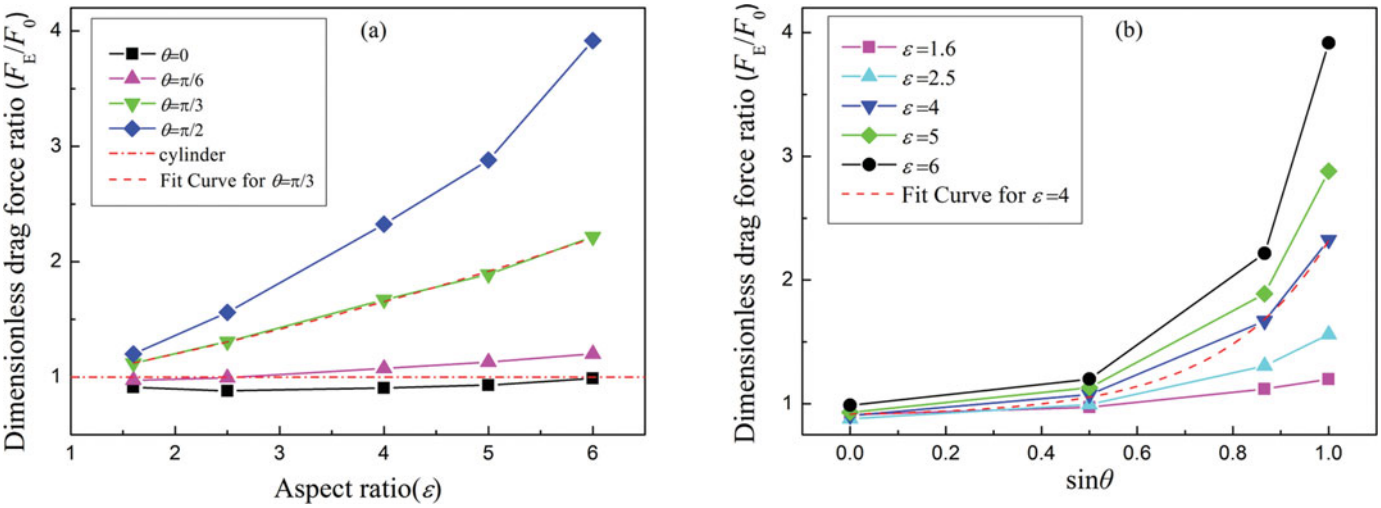

FIG. 3. The correction factor $C_{E,F}$ of dimensionless drag force between elliptical and circular fibers ((a): vs. ε; (b): vs. θ)v.

This is because the orientation angle θ directly determines the windward area when the cross-sectional shape of the elliptical fiber is given for a given ε; the larger θ is, the larger the windward area is, and the larger F_E is. From Figure 3, it is found that the correction factor of the dimensionless drag force F_E can be approximately expressed by a quadratic polynomial of ε if θ is fixed: $C_{E,F} = B_1 \cdot \varepsilon^2 + B_2 \cdot \varepsilon + B_3$. If ε is fixed, the relationship between $C_{E,F}$ and $\sin\theta$ is roughly exponentially formulated: $C_{E,F} = A_1 \cdot \exp(-\sin\theta/A_2) + A_3$. With a comprehensive consideration on the effects of θ and ε, we assume that the correction factor of the pressure drop for the elliptical fiber is formulated by $C_{E,F} = A_1 \cdot \exp(-\sin\theta/A_2) + A_3$, where the parameters A_1, A_2, A_3 are regarded as the quadratic polynomial of ε:

$$C_{E,F} = F_E/F_0 = \left(\beta_1 \cdot \varepsilon^2 + \beta_2 \cdot \varepsilon + \beta_3\right) \cdot \exp\left(-\sin\theta/(\beta_4 \cdot \varepsilon^2 + \beta_5 \cdot \varepsilon + \beta_6)\right) + \beta_7 \cdot \varepsilon^2 + \beta_8 \cdot \varepsilon + \beta_9. \quad [19]$$

Based on the simulation results of the LB-CA model under different conditions (Figure 3), each coefficient is estimated by the LMA. The best parameter set is gained from the minimization as follows: $\beta_1 = -1.115 \times 10^{-3}$, $\beta_2 = 9.081 \times 10^{-3}$, $\beta_3 = -7.828 \times 10^{-4}$, $\beta_4 = 2.536 \times 10^{-3}$, $\beta_5 = -4.170 \times 10^{-3}$, $\beta_6 = -2.305 \times 10^{-1}$, $\beta_7 = 1.315 \times 10^{-2}$, $\beta_8 = -8.635 \times 10^{-2}$, and $\beta_9 = 1.051$. It is seen that $C_{E,F}$ is approximately equal to 1 for different θ when $\varepsilon = 1$.

We further compare the predictions of Equation (19) with the results of Kirsh (2011), as concluded in Table 1. The relative error between $C_{E,F}$ and result of Kirsh is less than 10%. The good agreement between them proves that the correction factor formulated by Equation (19) is accurate enough to calculate the dimensionless drag force on elliptical fibers in a simple way.

CAPTURE EFFICIENCY

Three kinds of particles are chosen to represent three capture mechanisms respectively and their trajectories are shown in Figure 4. The motion of submicron particles is dominated by random Brownian diffusion. Particle trajectory is relatively disordered and particles could move to any position of the fiber surface (Figure 4a). When interception capture mechanism is predominant, the trajectories of particles in the flow field almost follow the streamline (Figure 4b). The large particles with great inertia often deviate from streamline during their motion process and collide with the windward side of fibers then get captured (Figure 4c). In interception and inertial impaction mechanisms, the Brownian force is assumed to be 0, leading to $Pe = \infty$. In addition, the particle velocity is equal to local fluid velocity and St is set to be 0 when the interception mechanism is dominated,

TABLE 1
Comparison of $C_{E,F}$ and results of Kirsh ($\alpha = 25.5\%$)

Aspect ratio, ε	Orientation angle, θ	$C_{E,F}$	Kirsh (2011)	Relative error
2	0	0.937	0.854	9.72%
2	$\pi/6$	0.984	0.973	1.13%
2	$\pi/3$	1.190	1.259	5.48%
2	$\pi/2$	1.397	1.427	2.10%

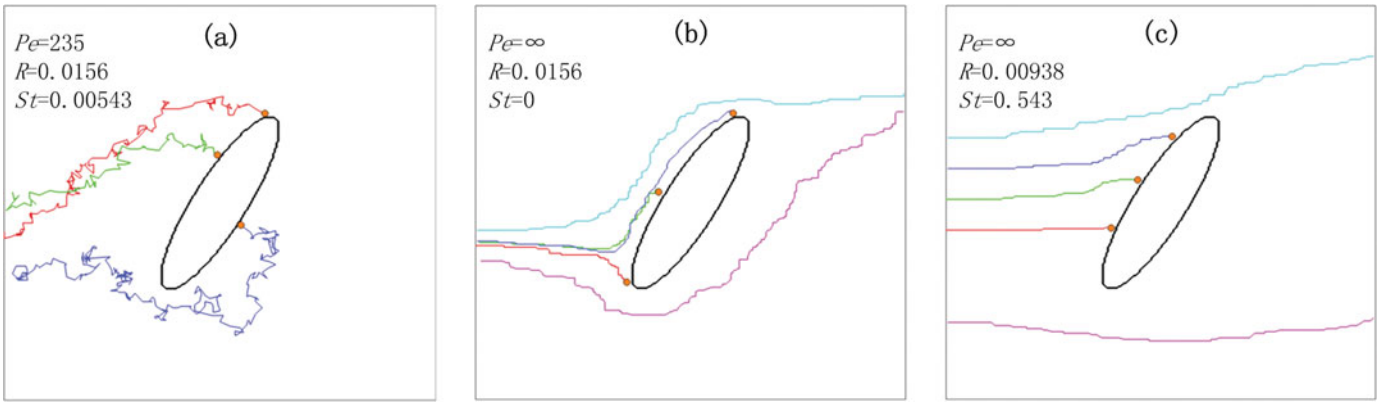

FIG. 4. Particle trajectories in different mechanisms: (a) diffusion; (b) interception; (c) inertial impaction; $\varepsilon = 4$, $\theta = \pi/3$.

which excludes the effects of diffusion and inertial impaction mechanisms. The capture efficiency of these particles for single circular fiber due to different capture mechanisms shows that the three kinds of particles are reasonable to represent three capture mechanisms.

The Effect of Fiber Packing Density on Capture Efficiency

Similar to the pressure drop discussed in the former section, the effect of packing density on the capture efficiency is analyzed first (Figure 5). It is also found that the ratio of capture efficiency for elliptical fibers to that of circular fiber almost remains unchanged as the packing density changes if the aspect ratio and orientation angle are fixed.

Diffusional Capture Efficiency

The effect of orientation angle θ on diffusional capture efficiency is investigated first. It is found that the diffusional capture efficiency of elliptical fibers $\eta_{E,D}$ is almost determined by ε and independent of θ. For example, $\eta_{E,D}$ approximately equals to 9% for arbitrary θ when $\varepsilon = 1.6$ and $Pe = 235$. Then, the diffusional capture efficiencies with different ε are shown in Figure 6. It is clear that the capture area of the elliptical fiber enlarges as ε increases, which finally leads to the increase of the diffusional capture efficiency; furthermore, it is found that the diffusional capture efficiency scales nearly linearly as ε. At this point, we assume that the correction factor, $C_{E,D} = \eta_{E,D}/\eta_{0,D}$, is proportional to ε, where the diffusional capture efficiency of circular fiber ($\eta_{0,D}$) used here is from the classical expression of Stechkina and Fuchs (1966):

$$\eta_{0,D} = 2.9 Ku^{-1/3} Pe^{-2/3} + 0.62 Pe^{-1},$$
$$Ku = -0.5 \ln \alpha - 0.75 + \alpha - 0.25\alpha^2. \quad [20]$$

Through simple linear fitting, the expression of $C_{E,D}$ is obtained as follows:

$$C_{E,D} = 0.06592\varepsilon + 0.95243. \quad [21]$$

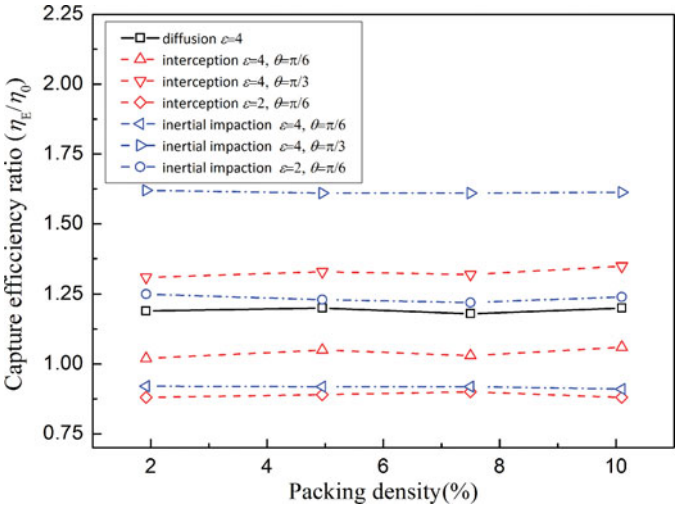

FIG. 5. Capture efficiency ratio of elliptical to circular fiber vs. packing density.

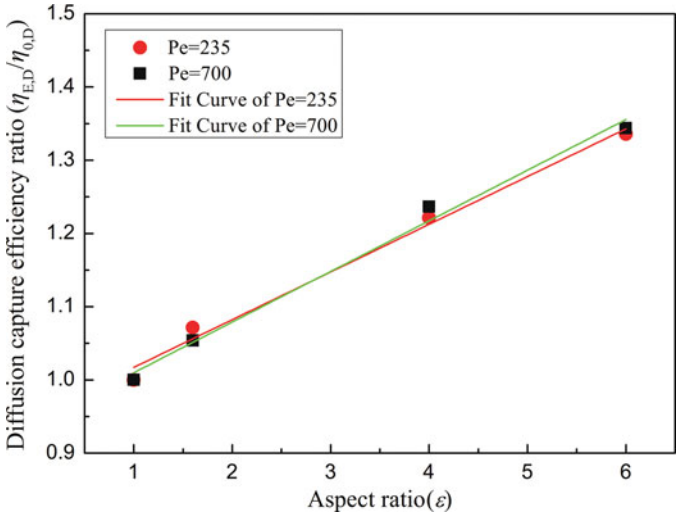

FIG. 6. Diffusional capture efficiency ratio ($\eta_{E,D}/\eta_{0,D}$).

TABLE 2
Diffusional capture efficiency with different ε ($\eta_{E,D}/\eta_{0,D}$), where $\eta_{Raynor,D}$ is the prediction of Regan and Raynor (2009)

Pe	ε	LB-CA	$C_{E,D}$	$\eta_{Raynor,D}/\eta_{0,D}$	Relative error
235	1.6	1.071	1.058	1.024	3.32%
235	4	1.221	1.216	1.167	4.20%
235	6	1.336	1.348	1.286	4.82%
700	1.6	1.054	1.058	1.025	3.22%
700	4	1.237	1.216	1.175	3.49%
700	6	1.344	1.348	1.300	3.69%

Obviously, $C_{E,D}$ is independent to θ and approximately equal to 1 when $\varepsilon = 1$.

Table 2 presents the comparison between simulation results from the LB-CA and empirical prediction by Equation (21), showing that they fit very well and the correlation coefficient reaches 0.995. Regan and Raynor (2009) also developed a semi-empirical expression for the diffusional capture efficiency of single elliptical fiber. However, their formula, which has 12 empirical parameters, is much more complicated than Equation (21). Table 2 also demonstrates that there is only a little difference between Equation (21) and Regan & Raynor formula. The relative error is defined as: $(C_{E,D}\text{-}\eta_{Raynor,D}/\eta_{0,D})/(\eta_{Raynor,D}/\eta_{0,D})$. It is considered that the correction factor $C_{E,D}$ can accurately account for the change of diffusional capture efficiency caused by the elliptical fiber shape.

Interception Capture Efficiency

With the increase of particle size, the Brownian diffusion ability of particle gradually weakens, and then interception effect gradually becomes dominant. Obviously, when interception mechanism dominates the filtration, the effects of R ($=d_p/d_f = d_p/(ab)^{1/2}$) as well ε and θ on capture efficiency should be taken into account. Figure 7 presents the ratio of interception capture efficiency ($C_{E,R} = \eta_{E,R}/\eta_{0,R}$) between the elliptical fiber and the circular fiber with the same packing density while different ε, θ, and R. The analytical expression of the interception capture efficiency for circular fiber ($\eta_{0,R}$) used here is from Lee and Liu (1982):

$$\eta_{0,R} = \frac{1+R}{2Ku}\left[2\ln(1+R) - 1 + \alpha + \left(\frac{1}{1+R}\right)^2\left(1-\frac{\alpha}{2}\right) - \frac{\alpha}{2}(1+R)^2\right], \quad [22]$$

where $Ku = -0.5\ln\alpha - 0.75 + \alpha - 0.25\alpha^2$. From Figure 7 it is found that R has only slight influence on the correction factor of interception capture efficiency, which is because the formula (Equation (22)) has adequately considered the influence of R on the interception capture efficiency. Therefore, we only need to consider the effect of ε and θ on the correction factor of the interception efficiency.

It is found that the relationship between $C_{E,R}$ and $\sin\theta$ is roughly exponential from Figure 7, that is, $C_{E,R} = A_1 \times \exp(-\sin\theta/A_2) + A_3$, when ε is fixed. However, when θ is fixed, the drag force can be formulated by the quadratic polynomial of ε as follows: $B_1 \cdot \varepsilon^2 + B_2 \cdot \varepsilon + B_3$. Representing A_1, A_2, and A_3 as the quadratic polynomial of ε, we obtain

$$C_{E,F} = \left(\beta_1 \cdot \varepsilon^2 + \beta_2 \cdot \varepsilon + \beta_3\right) \cdot \exp(-\sin\theta / (\beta_4 \cdot \varepsilon^2 + \beta_5 \cdot \varepsilon + \beta_6)) + \beta_7 \cdot \varepsilon^2 + \beta_8 \cdot \varepsilon + \beta_9. \quad [23]$$

Using the LMA to fit these LB-CA simulation results, the best parameter set is obtained as follows: $\beta_1 = 1.324 \times 10^{-3}$, $\beta_2 = 1.269 \times 10^{-2}$, $\beta_3 = -1.533 \times 10^{-2}$, $\beta_4 = -5.573 \times 10^{-3}$, $\beta_5 = 6.856 \times 10^{-2}$, $\beta_6 = 1.914 \times 10^{-1}$, $\beta_7 = 1.055 \times 10^{-1}$, $\beta_8 = -6.133 \times 10^{-1}$, and $\beta_9 = 1.570$. Table 3 demonstrates the comparison between simulation results from the LB-CA and Equation (23), and the relative errors are constrained within 8%. The results predicted by the model (Raynor 2008) are also presented in Table 3. In the semi-empirical model of Raynor, the interception capture efficiency is attained by dividing the distance between the centerline and limiting streamline by the radius ($(ab)^{1/2}/2$) of a circular fiber. Actually, the windward area

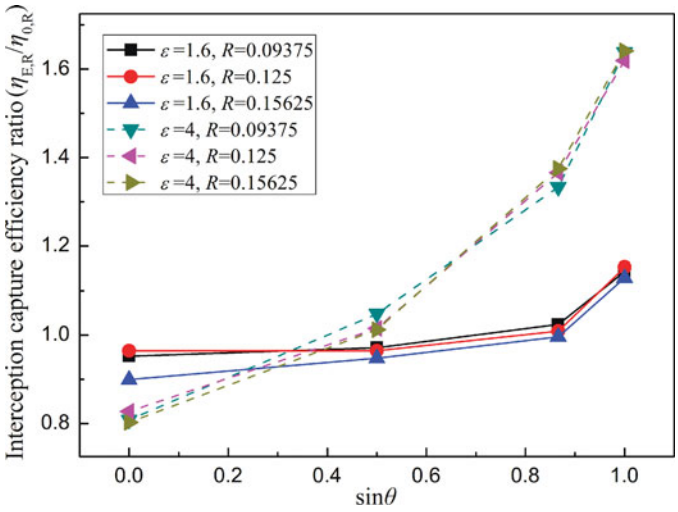

FIG. 7. Interception capture efficiency ratio ($\eta_{E,R}/\eta_{0,R}$).

TABLE 3
Interception capture efficiency ($\eta_{E,R}/\eta_{0,R}$), where $\eta_{Raynor,E}$ is the prediction of Raynor (2008)

ε	θ	LB-CA	$C_{E,R}$	$\eta_{Raynor,E}/\eta_{0,R}$
1.6	0	0.939	0.867	0.639
1.6	$\pi/6$	0.961	0.907	0.881
1.6	$\pi/3$	1.043	1.030	1.084
1.6	$\pi/2$	1.175	1.132	1.181
4	0	0.815	0.861	0.358
4	$\pi/6$	1.025	1.018	0.921
4	$\pi/3$	1.358	1.370	1.391
4	$\pi/2$	1.633	1.612	1.654

depends on the length of minor axes when $\theta = 0$ and the length of major axes when $\theta = \pi/2$. Obviously, $b < (ab)^{1/2} < a$ and the gap between the three values increases with ε. That is why, the LB-CA results are higher than these of Raynor estimation when $\theta = 0$, while lower when $\theta = \pi/2$.

Inertial Impaction Capture Efficiency

Based on the LB-CA simulation, we find that ε, θ, and R have the synergetic effects on the impaction efficiency. Figure 8 demonstrates the changes of impaction efficiency as a function of ε, θ, and R, where the expression of $\eta_{0,I}$ for circular fiber is from Brown (1993)

$$\eta_{0,I} = \frac{St \cdot \left[(29.6 - 28\alpha^{0.62})R^2 - 27.5R^{2.8}\right]}{2Ku^2}. \qquad [24]$$

From Figure 8, it is found that (1) the impaction capture efficiency of elliptical fiber, $\eta_{E,I}$, increases as θ; (2) the growth rate of $\eta_{E,I}$ depends on R. The bigger R is, the faster the efficiency

TABLE 4
Inertial impaction capture efficiency ($\eta_{E,I}/\eta_{0,I}$)

ε	θ	$R = d_p/d_f$	LB-CA	$C_{E,I}$	Relative error
1.6	0	0.09375	0.943	0.923	−2.00%
1.6	0	0.125	0.905	0.864	−4.40%
1.6	0	0.15625	0.853	0.789	−7.26%
1.6	$\pi/6$	0.09375	0.966	0.975	1.03%
1.6	$\pi/6$	0.125	0.966	0.964	−0.15%
1.6	$\pi/6$	0.15625	0.941	0.959	2.00%
1.6	$\pi/3$	0.09375	1.019	1.032	1.31%
1.6	$\pi/3$	0.125	1.053	1.076	2.21%
1.6	$\pi/3$	0.15625	1.089	1.159	6.45%
1.6	$\pi/2$	0.09375	1.132	1.066	−5.74%
1.6	$\pi/2$	0.125	1.178	1.147	−2.64%
1.6	$\pi/2$	0.15625	1.208	1.290	6.83%
4	0	0.09375	0.845	0.878	3.81%
4	0	0.125	0.684	0.729	6.71%
4	0	0.15625	0.545	0.541	−0.10%
4	$\pi/6$	0.09375	1.057	1.007	−4.75%
4	$\pi/6$	0.125	1.013	0.979	−3.42%
4	$\pi/6$	0.15625	0.941	0.966	2.71%
4	$\pi/3$	0.09375	1.132	1.147	1.39%
4	$\pi/3$	0.125	1.291	1.258	−2.60%
4	$\pi/3$	0.15625	1.485	1.465	−1.35%
4	$\pi/2$	0.09375	1.208	1.234	2.20%
4	$\pi/2$	0.125	1.392	1.434	3.02%
4	$\pi/2$	0.15625	1.842	1.793	−2.65%

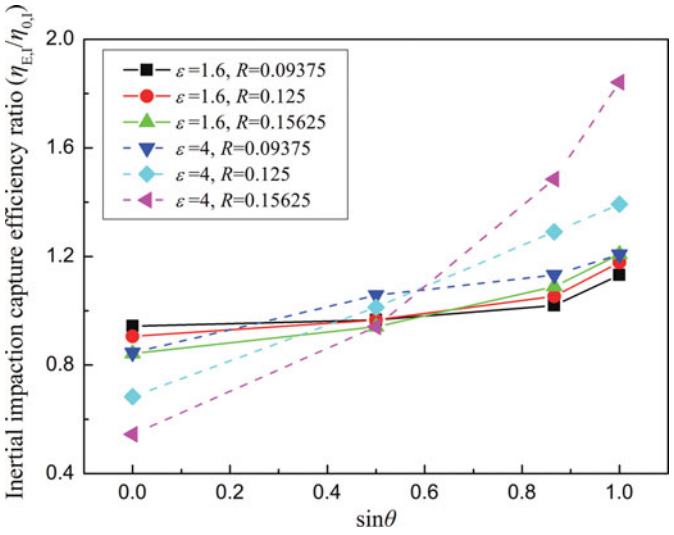

FIG. 8. Inertial impaction capture efficiency ratio ($\eta_{E,I}/\eta_{0,I}$).

increases; (3) ε and θ determine together the windward area of the elliptical fiber, which has a significant influence on the impaction efficiency. $\eta_{E,I}/\eta_{0,I} < 1$ when $\theta < 30^\circ$, $\eta_{E,I}/\eta_{0,I} \approx 1$ when $\theta = 30^\circ$; while $\eta_{E,I}/\eta_{0,I}$ 1 when θ 30°; (4) the inertial impaction capture efficiency of the elliptical fiber may be lower than that of the circular fiber when the elliptical cross section is slimmer (with larger ε) and the major axis is closer to the incoming flow. However, whatever ε is, $\eta_{E,I}$ is usually larger than $\eta_{E,0}$ when θ is larger than 30°; (5) the effect of the interception parameter on $C_{E,I}$ when $\varepsilon = 1.6$ is less than the cases when $\varepsilon = 4$. It is attributed to the shape effect. A larger ε means a slimmer elliptical fiber and then a larger friction surface area and windward area of the fiber, which has greater impact on the inertial impaction collection efficiency.

Similarly, we use the LMA to explore the expression of $C_{E,I}(=\eta_{E,I}/\eta_{0,I})$, which is finally obtained as follows:

$$C_{E,I} = (\beta_1 \cdot R^2 + \beta_2 \cdot R + \beta_3 + \exp((\beta_4 \cdot R^2 + \beta_5 \cdot R + \beta_6) \times \sin(\beta_7 \cdot \theta + \beta_8))) \cdot \varepsilon + \beta_9. \quad [25]$$

In the expression, $\beta_1 = 3.105$; $\beta_2 = -7.918 \times 10^{-1}$; $\beta_3 = -9.364 \times 10^{-1}$; $\beta_4 = -14.065$; $\beta_5 = 1.433$; $\beta_6 = -6.453 \times 10^{-1}$; $\beta_7 = 1.306$; $\beta_8 = -3.896$; $\beta_9 = 9.554 \times 10^{-1}$. Table 4 demonstrates the fitting results and the simulation results, between which the relative errors are very small (<8%). Factually, the correlation coefficient is 0.988. It is noted that there is no analytical solution for the impaction capture efficiency of elliptical fiber up to now.

PERFORMANCE OF ELLIPTICAL FIBERS WHEN DIFFERENT CAPTURE MECHANISMS ARE PREDOMINANT

A good filter should exhibit high capture efficiency and low-pressure drop. The quality factor (or the figure of merit) is

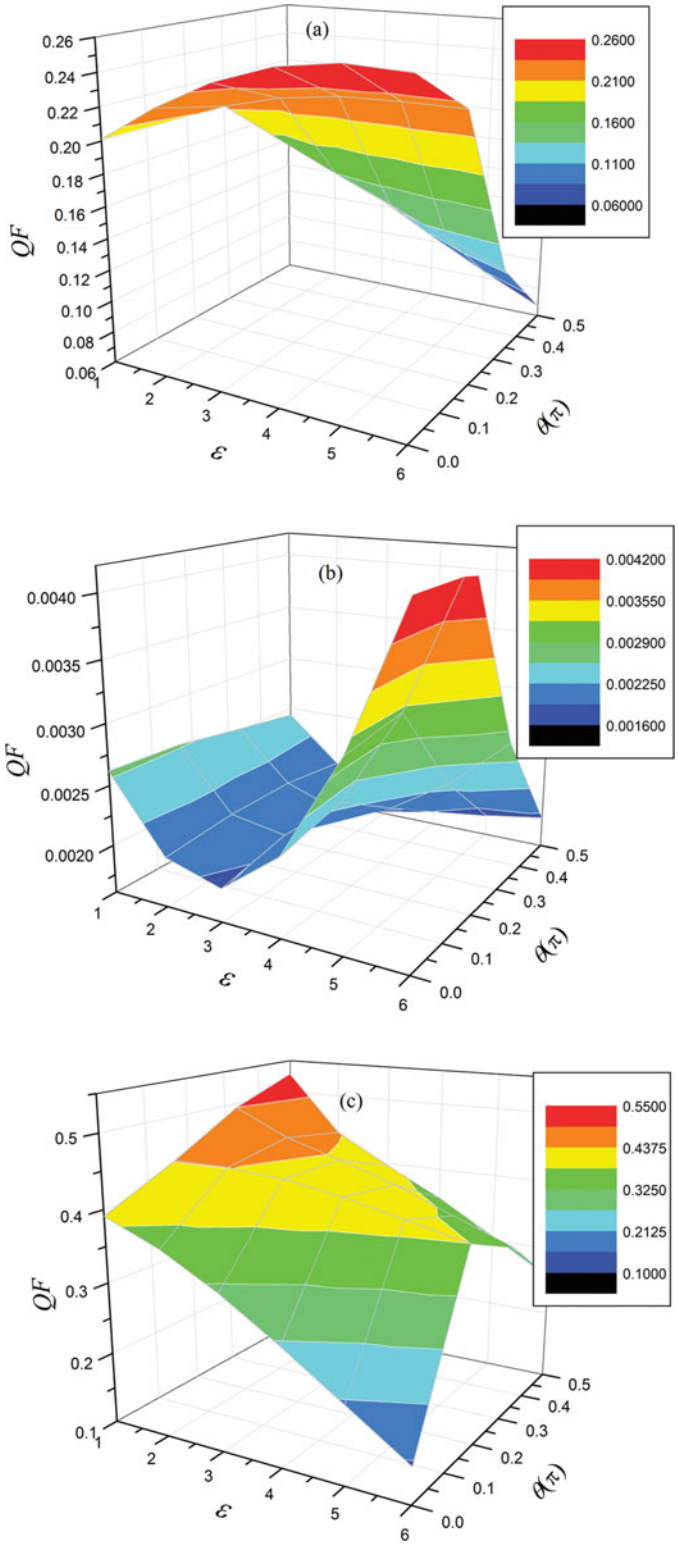

FIG. 9. Quality factor of elliptical fiber with different ε and θ when (a) Brownian diffusion, (b) interception, and (c) inertial impaction are dominated.

usually used to measure the performance of fibrous filters, which is defined as $-ln(P)/\Delta p$, could be derived according to Wang and Pui (2009):

$$QF = \frac{\eta}{(1-\alpha)\cdot(2F/\mathrm{Re})\cdot(\rho u^2/2)}, \qquad [26]$$

where P is the penetration, Re $(=(ab)^{1/2}u_0/\nu)$ is the Reynolds number, and η is the single-fiber capture efficiency.

Figure 9 presents the performances of elliptical fiber with various ε and θ due to different capture mechanisms. It demonstrates that ε and θ obviously affect the quality factor of elliptical fiber in different operation conditions. Obviously, pressure drop increases faster than capture efficiency in the case of large ε and θ, leading to a fall in the quality factor. For small particles where Brownian diffusion is predominant, the elliptical fiber performs better when ε is larger and $\theta = 0$ (Figure 9a). When collecting intermediate particles dominated only by interception mechanism, the quality factor increases almost with ε. However, a larger ε would lead to a higher pressure drop, which has a deleterious effect on the quality factor. Figure 9b shows that it is better to restrain θ within $(0, 0.15\pi)$ when ε is larger to keep higher quality factor. When the elliptical fiber is used to capture large particles where inertial impaction is the predominant mechanism, its capture efficiency is very sensitive to the windward area. For a fixed ε, the windward area is only determined by θ and gets its maximum when $\theta = \pi/2$. Although the filter has the highest capture efficiency when the major axis is perpendicular to the direction of inlet flow, the pressure drop also gets its maximum at this point. The competition relation contributes to a relatively lower quality factor especially for a larger ε. Figure 9c shows that the elliptical fiber usually performs worse than the circular fiber ($\varepsilon = 1$) for the filtration large particles.

CONCLUSION

This article used the LB-CA model to simulate the filtration process of elliptical fibers. We calculated the pressure drop of the system with different fiber orientation angles and aspect ratios and capture efficiency due to various capture mechanisms, then compared them with these of the circular fibers. The results showed that the elliptical fiber has higher capture efficiency for these Brownian-diffusion-dominated small particles because the elliptical fiber has larger capture area than the circular fiber. Moreover, the diffusional capture efficiency is almost proportional to the aspect ratio, while it is independent of the orientation angle of fiber. When interception or inertial impaction mechanism is dominant, the most important influencing factor to capture efficiency is the windward area determined by ε and θ. The impaction capture efficiency of larger particles also depends on R, that is, the larger R is, the faster capture efficiency increases. The collection efficiency of interception- or impaction-dominated particles by elliptical fiber is almost higher than that by circular fiber when $\theta > 30^\circ$, while the capture efficiency of elliptical fiber is lower when the major axis is more parallel to the incoming flow.

In this article, the Levenberg–Marquardt algorithm was introduced to obtain a series of correction factors for the pressure drop and capture efficiency of the elliptical fiber based on the existing formulas of circular fiber. It is found that the correction factors for the pressure drop and capture efficiency are nearly independent of the packing density. These fitted correction factors have more concise expressions than some available semi-empirical models, and they exhibit reasonable predictions and could be applied in engineering. This article provides for the first time an available expression for the impaction capture efficiency of elliptical fiber. Also, from these correction factors, a clear relationship between the filtration performance of elliptical fiber and that of circular fiber is presented. It is also noted that the Levenberg–Marquardt algorithm, which is utilized to fit some well-organized LB-CA simulations for quantitative prediction of the filtration performance of elliptical fiber, provides references for the simulation and modeling of the filtration processes of other noncircular fibers (i.e., rectangular and square fibers) and dust-loaded fibers.

Based on these empirical models for pressure drop and capture efficiency, the quality factor as a function of aspect ratio and located angle were investigated. It is found that the elliptical fiber with an orientation angle of 0 is better when capturing small particles; when interception mechanism dominates, it is better to restrain the orientation angle between 0 and 0.15π; when capturing particles with large inertia, the elliptical fiber is not at advantage of the quality factor over the circular fiber. The observations are capable of optimizing fiber arrangement under different working conditions.

NOMENCLATURE

α	packing density of fibers
β	parameters in correction factor
ε	aspect ratio
θ	orientation angle
Re	Reynolds number
Ku	Kuwabara number
Pe	Peclet number
St	Stokes number
ΔP	pressure drop of fibrous filter
F_0	dimensionless drag force in per unit length of circular fiber
F_E	dimensionless drag force in per unit length of elliptical fiber
$\eta_{\mathrm{E,D}}$	diffusional capture efficiency of elliptical fiber
$\eta_{0,\mathrm{D}}$	diffusional capture efficiency of circular fiber
$\eta_{\mathrm{E,R}}$	interception capture efficiency of elliptical fiber
$\eta_{0,\mathrm{R}}$	interception capture efficiency of circular fiber
$\eta_{\mathrm{E,I}}$	inertial impaction capture efficiency of elliptical fiber
$\eta_{0,\mathrm{I}}$	inertial impaction capture efficiency of circular fiber
$C_{\mathrm{E,F}}$	correction factor for pressure drop of elliptical fiber

$C_{E,D}$ correction factor for diffusional capture efficiency of elliptical fiber
$C_{E,R}$ correction factor for interception capture efficiency of elliptical fiber
$C_{E,I}$ correction factor for inertial impaction capture efficiency of elliptical fiber

FUNDING

This study was financially supported by the National Natural Science Foundation of China (51276077, 51390494), Program for New Century Excellent Talents in University (NCET-10–0395), and National Key Basic Research and Development Program (2010CB227004 and 2013CB228504).

REFERENCES

Adamiak, K. (1999). Viscous Flow Model for Charged Particle Trajectories Around a Single Square Fiber in an Electric Field. *IEEE T. Ind. Appl.*, 35:352–358.

Bhatnagar, P. L., Gross, E. P., and Krook M. (1954). A Model for Collision Processes in Gases. I: Small Amplitude Processes in Charged and Neutral One-Component System. *Phys. Rev.*, 94:511–525.

Brown, R. C. (1984). A Many-Fibre Model of Airflow Through a Fibrous Filter. *J. Aerosol Sci.*, 15:583–593.

Brown, R. C. (1993). *Air Filtration: An Integrated Approach to the Theory and Applications of Fibrous Filters*. Pergamon Press, New York.

Cao, Y., Cheung, C., and Yan, Z. (2004). Numerical Study of an Electret Filter Composed of an Array of Staggered Parallel Rectangular Split-Type Fibers. *Aerosol. Sci. Technol.*, 38:603–618.

Cheung, C., Cao, Y., and Yan, Z. (2005). Numerical Model for Particle Deposition and Loading in Electret Filter with Rectangular Split-Type Fibers. *Comput. Mech.*, 35:449–458.

Dhaniyala, S. (1999). An Asymmetrical, Three-Dimensional Model for Fibrous Filters. *Aerosol Sci. Technol.*, 30:333–348.

Dunnett, S., and Clement, C. (2012). Numerical Investigation into the Loading Behaviour of Filters Operating in the Diffusional and Interception Deposition Regimes. *J. Aerosol Sci.*, 53:85–99.

Fardi, B., and Liu, B. Y. H. (1992a). Flow Field and Pressure Drop of Filters with Rectangular Fibers. *Aerosol Sci. Technol.*, 17:36–44.

Fardi, B., and Liu, B. Y. H. (1992b). Efficiency of Fibrous Filters with Rectangular Fibers. *Aerosol Sci. Technol.*, 17:45–58.

Guo, Z. L., Zheng, C. G., and Shi, B. C. (2002). Non-Equilibrium Extrapolation Method for Velocity and Pressure Boundary Conditions in the Lattice Boltzmann Method. *Chinese Phys.*, 11:366–374.

Happel, J. (1959). Viscous Flow Relative to Arrays of Cylinders. *AIChE. J.*, 5:174–177.

Homonoff, E., and Dugan, J. (2001). Specialty Fibers for Filtration Applications, in *Advances in Filtration and Separation Technology*, vol. 15, American Filtration and Separations Society, Falls Church, VA (CD-ROM).

Hosseini, S., and Tafreshi, H. V. (2010a). 3-D Simulation of Particle Filtration in Electrospun Nanofibrous Filters. *Powder Technol.*, 201:153–160.

Hosseini, S., and Tafreshi, H. V. (2010b). Modeling Particle Filtration in Disordered 2-D Domains: A Comparison with Cell Models. *Sep. Purif. Technol.*, 74(2):160–169.

Hosseini, S., and Tafreshi, H. V. (2011). On the Importance of Fibers' Cross-Sectional Shape for Air Filters Operating in the Slip Flow Regime. *Powder Technol.*, 212:425–431.

Kasper, G., Schollmeier, S., and Meyer, J. (2010). Structure and Density of Deposits Formed on Filter Fibers by Inertial Particle Deposition and Bounce. *J. Aerosol Sci.*, 41:1167–1182.

Kirsch, A., and Fuchs, N. (1967). Studies on Fibrous Aerosol Filters. II. Pressure Drops in Systems of Parallel Cylinders. *Ann. Occup. Hyg.*, 10:23–30.

Kirsch, A., and Fuchs, N. (1968). Studies on Fibrous Aerosol Filters. III. Diffusional Deposition of Aerosols in Fibrous Filters. *Ann.Occup. Hyg.*, 11: 299.

Kirsh, V. (2011). Stokes Flow and Deposition of Aerosol Nanoparticles in Model Filters Composed of Elliptic Fibers. *Colloid J.*, 73:345–351.

Kuwabara, S. (1959). The Forces Experienced by Randomly Distributed Parallel Circular Cylinders or Spheres in a Viscous Flow at Small Reynolds Numbers. *J. Phys. Soc. Jpn.*, 14:527.

Lee, K. W., and Liu, B. Y. H. (1981). Experimental Study of Aerosol Filtration by Fibrous Filters. *Aerosol Sci. Technol.*, 1:35–46.

Lee, K. W., and Liu, B. Y. H. (1982). Theoretical Study of Aerosol Filtration by Fibrous Filters. *Aerosol Sci. Technol.*, 1:147–161.

Liu, Z. G., and Wang, P. K. (1997). Pressure Drop and Interception Efficiency of Multifiber Filters. *Aerosol Sci. Technol.*, 26:313–325.

Masliyah, J. H. (1975). Aerosol Removal by Diffusion and Interception in Mats of Elliptic Fibres. *Can. J. Chem. Eng.*, 53:568–571.

Maze, B., Vahedi Tafreshi, H., Wang, Q., and Pourdeyhimi, B. (2007). A Simulation of Unsteady-State Filtration via Nanofiber Media at Reduced Operating Pressures. *J. Aerosol Sci.*, 38:550–571.

More, J. (1978). The Levenberg–Marquardt Algorithm: Implementation and Theory, in *Numerical Analysis*, vol. 630, G. A. Watson, ed., ISBN 978-3-540-08538-6, Springer, Berlin , pp. 105–116.

Ouyang, M., and Liu, B. Y. H. (1998). Analytical Solution of Flow Field and Pressure Drop for Filters with Rectangular Fibers. *J. Aerosol Sci.*, 29:187–196.

Qian, Y. H., D'Humieres, D., and Lallemand, P. (1992). Lattice BGK Models for Navier–Stokes Equation. *Europhys. Lett.*, 17:479–484.

Raynor, P. C. (2002). Flow Field and Drag for Elliptical Filter Fibers. *Aerosol Sci. Technol.*, 36:1118–1127.

Raynor, P. C. (2008). Single-Fiber Interception Efficiency for Elliptical Fibers. *Aerosol Sci. Technol.*, 42:357–368.

Regan, B. D., and Raynor, P. C. (2009). Single-Fiber Diffusion Efficiency for Elliptical Fibers. *Aerosol Sci. Technol.*, 43:533–543.

Sanchez, J. R., Rodriguez, J., Alvaro, A., and Estevez, A. (2007). The Capture of Fly ash Particles Using Circular and Noncircular Cross-Section Fabric Filters. *Environ. Prog.*, 26:50–58.

Stechkina, I., and Fuchs, N. (1966). Studies on Fibrous Aerosol Filters. I. Calculation of Diffusional Deposition of Aerosols in Fibrous Filters. *Ann. Occup. Hyg.*, 9:59–64.

Stechkina, I., Kirsch, A., and Fuchs, N. (1969). Studies on Fibrous Aerosol Filters. IV. Calculation of Aerosol Deposition in Model Filters in the Range of Maximum Penetration. *Ann. Occup. Hyg.*, 12:1–8.

Tahir, M., and Tafreshi, H. V. (2009). Influence of Fiber Orientation on the Transverse Permeability of Fibrous Media. *Phys. Fluids.*, 21:083604.

Ushe, Z. (1993). The Effect of Different Shaped Cross-Sectional Microfibers on Filtration, in *Advances in Filtration and Separation Technology*, vol. 7, W. W. Leung, ed., pp. 146–147.

Wang, C. (1996). Stokes Flow Through an Array of Rectangular Fibers. *Int. J. Multiphas. Flow.*, 22:185–194.

Wang, H., Zhao, H., Guo, Z., He, Y., and Zheng, C. (2013). Lattice Boltzmann Method for Simulations of Gas-Particle Flows over a Backward-Facing Step. *J. Comput. Phys.*, 239:57–71.

Wang, H., Zhao, H., Guo, Z., and Zheng, C. (2012a). Numerical Simulation of Particle Capture Process of Fibrous Filters Using Lattice Boltzmann Two-Phase Flow Model. *Powder Technol.*, 227:111–122.

Wang, J., and Pui, D. Y. H. (2009). Filtration of Aerosol Particles by Elliptical Fibers: A Numerical Study. *J. Nanopart. Res.*, 11:185–196.

Wang, W., Xie, M., and Wang, L. (2012b). An Exact Solution of Interception Efficiency Over an Elliptical Fiber Collector. *Aerosol Sci. Technol.*, 46:843–851.

William, A., and Bobby, M. (1995). Deep Grooved Polyester Fiber for Wet Lay Applications. *Tappi J.*, 78:139–142.

Zhu, C., Lin, C. H., and Cheung, C. S. (2000). Inertial Impaction-Dominated Fibrous Filtration with Rectangular or Cylindrical Fibers. *Powder Technol.*, 112:149–162.